4D printed snake-like biomimetic soft robots

Xingcheng Ou[1]· Jiaqi Huang[1]· Dantong Huang[1]· Xiaohong Li[1]· Guoliang Chen[1]· Yabin Yang[1]· Ran Bi[1]· Yu Sheng[1]·Shuang-Zhuang Guo[1]*

E-mail: guoshzh3@mail.sysu.edu.cn
1 Guangzhou Key Laboratory of Flexible Electronic Materials and Wearable Devices, Guangdong Engineering Technology Research Centre for Functional Biomaterials, Key Laboratory for Polymeric Composite and Functional Materials of Ministry of Education, State Key Laboratory of Optoelectronic Materials and Technologies, School of Materials Science and Engineering, Sun Yat-sen University, Guangzhou 510275, P. R. China.

Abstract

Wireless millirobots, engineered to infiltrate the intricate vascular and cavitary network within living organisms, particularly within constricted and confined spaces, hold immense promise for the future of medical treatments. However, some robots, with their multifaceted and intricate designs, often grapple with motion and functionality issues when confronted with tight spaces characterized by small cross-sectional dimensions. Here, drawing inspiration from the high aspect ratio and undulating swimming patterns of snakes, a millimeter-scale snake-like robot alongside a sophisticated motion control strategy is designed and fabricated via combination of extrusion-based four-dimensional (4D) printing and magnetic-responsive intelligent functional inks. We also develop a sophisticated motion control strategy that enables the robots to perform various dynamic movements, such as undulating swimming, precise turns, graceful circular motions, and coordinated cluster movements, under diverse magnetic field variations. As a potential application, the snake robot can navigate and release drugs in a model coronary intervention vessel with tortuous channels and fluid filling. The novel design and promising applications of this snake robot are poised to emerge as invaluable tools in the realm of future medical surgeries and interventions.

Keywords· 4D Printing;· Magnetic Responsive Ink; Untethered Medical Soft Robot; Snake -like Robot; · Drug Delivery

Introduction

Wireless micro soft robots exhibit the remarkable ability to traverse intricate and confined environment with utmost delicacy, enabling access to anatomically intricate regions within the body, including blood vessels and lumen channels, for a spectrum of medical interventions [1, 2] such as targeted drug delivery [3–5], endoscopy [6, 7] and minimally invasive surgery [8, 9]. These robots hold the promise of detecting and excising tumors, precisely administering therapeutic payloads, and executing other vital medical tasks with unparalleled precision, all while minimizing disruption to the patient's physiological equilibrium [10, 11]. Conventional micro-robot actuators, encompassing elements like miniature motors and hydraulic mechanisms, often prove unwieldy due to their bulky nature and intricate connections, rendering them unfeasible for application within the restricted, confined domains inherent to medical contexts. The absence of physical tethers for power transmission in magnetic driven soft robots facilitates the design of robots with miniaturization [12], as well as their soft and flexible properties without damage to biological tissues [8]. In addition, the remote orchestration of magnetic fields offers a secure avenue of manipulating unrestrained soft robots in enclosed spaces within the human body [13]. Hence, the magnetic paradigm emerges as a potent candidate for bolstering the arsenal of surgical tools in the medical landscape.

In parallel to these advancements, biomimetic magnetic micro-robots have experienced rapid evolution, reflecting an array of intricate motions akin to their biological counterparts, encompassing crawling [14–16], leaping [17], rolling [18], and swimming [19, 20]. Notwithstanding these feats, a critical hurdle persists—the ingress and operation of these micro-robots within the challenging milieu of narrow, winding, and fluid-filled vascular networks (Fig. 1a). The resolution to this quandary lies in the strategic reduction of the robot's cross-sectional area vis-à-vis its confined surroundings. Within these restricted dimensions, the geometrical architecture of micro-robots inevitably gravitates toward simplicity, epitomized by configurations such as planar sheet [21–23], spherical entities [24], helical forms [25, 26], and filamentous structures [27, 28]. In particular, continuous robots with ferromagnetic tip filaments, whose bending can be controlled via remote manipulation of magnetic fields, have been developed[29–31]. These active continuous robots have demonstrated enhanced mobility for navigation

through blood vessels and the ability to deliver embolic agents to aneurysms. However, despite their efficacy, these guidewires and catheters, featuring both passive and active tips, are fundamentally limited by their tethered nature, relying on external push-and-pull mechanisms. Furthermore, their elongated structures, often exceeding a meter in length, exacerbate tissue friction, especially when navigating through narrow, convoluted blood vessels, making maneuverability challenging when highly twisted, bent, or wound.

To address this issue, another strategy is to develop tiny, wireless robots that can fully access and navigate in the blood vessels, thus replacing filament-like continuous robots. Efficient locomotion within intricate biological milieus mandates the microrobots to possess lateral dimensions markedly smaller than the cross-sectional area of the confined spaces, coupled with propulsion mechanisms that surmount the resistance of liquids. Drawing inspiration from the remarkable attributes of serpents – creatures endowed with elongated, sinuous bodies, multiple joints, a surplus of degrees of freedom, and a lack of limbs-researchers have sought to emulate their exceptional athleticism [32–34]. Serpents, by virtue of their lithe physiques, demonstrate unparalleled agility in negotiating confined domains, harnessing a succession of undulatory waves that propagate from head to tail within liquid environments, thus triumphing over hydrodynamic resistance and accomplishing rapid locomotion [35, 36]. Capitalizing on the biomechanics of serpentine movement and the innate qualities of their lithe forms, we propose the conceptualization of a biomimetic robot that mirrors the attributes of a snake – an entity characterized by its elongated, high aspect ratio structure. This bio-inspired creation holds the potential to venture into narrow conduits, traverse convoluted trajectories, and precisely administer pharmaceutical agents at predetermined locales within blood vessels. However, there are still huge challenges in designing, manufacturing, and manipulating these robots.

Additive manufacturing (AM), or three-dimensional (3D) printing, is an innovative manufacturing technique that creates 3D objects by adding materials layer by layer[37, 38]. In contrast to 3D printing, 4D printing creates objects capable of changing their shape or properties in response to specific external stimuli, such as temperature, humidity, light, current, or magnetic fields. 4D printing technology offers a variety of designs and options for soft robots' structures and magnetic pole distribution. These soft robots can be manufactured with high accuracy for any shape and structure by 4D printing technology, which enables them to be innovative and adaptable for various medical application. As a demonstration, we developed an open-source DIW 3D printing system and prepared a magnetic responsive intelligent ink which was a thixotropic paste with shear-yielding and shear-thinning properties, to directly print a snake robot, who was subsequently programmed to orchestrate oscillatory motion within a magnetic field-analogous to the undulations of snake locomotion. The dynamic magnetic field, engendered by a meticulously engineered 3D Helmholtz coil system, served as the conductor orchestrating the intricate choreography of the robotic snake's diverse movements, including swimming in a straight line, turning, circling, and performing group motion. Envisioned as a potential application, this elongated robotic serpent could seamlessly navigate a simulated coronary vessel system, swiftly and precisely accessing the designated destination for controlled drug delivery. In the grand scheme of things, this innovative serpent-inspired robot holds promise for reshaping the landscape of minimally invasive drug therapy, charting a course towards more effective and targeted medical interventions.

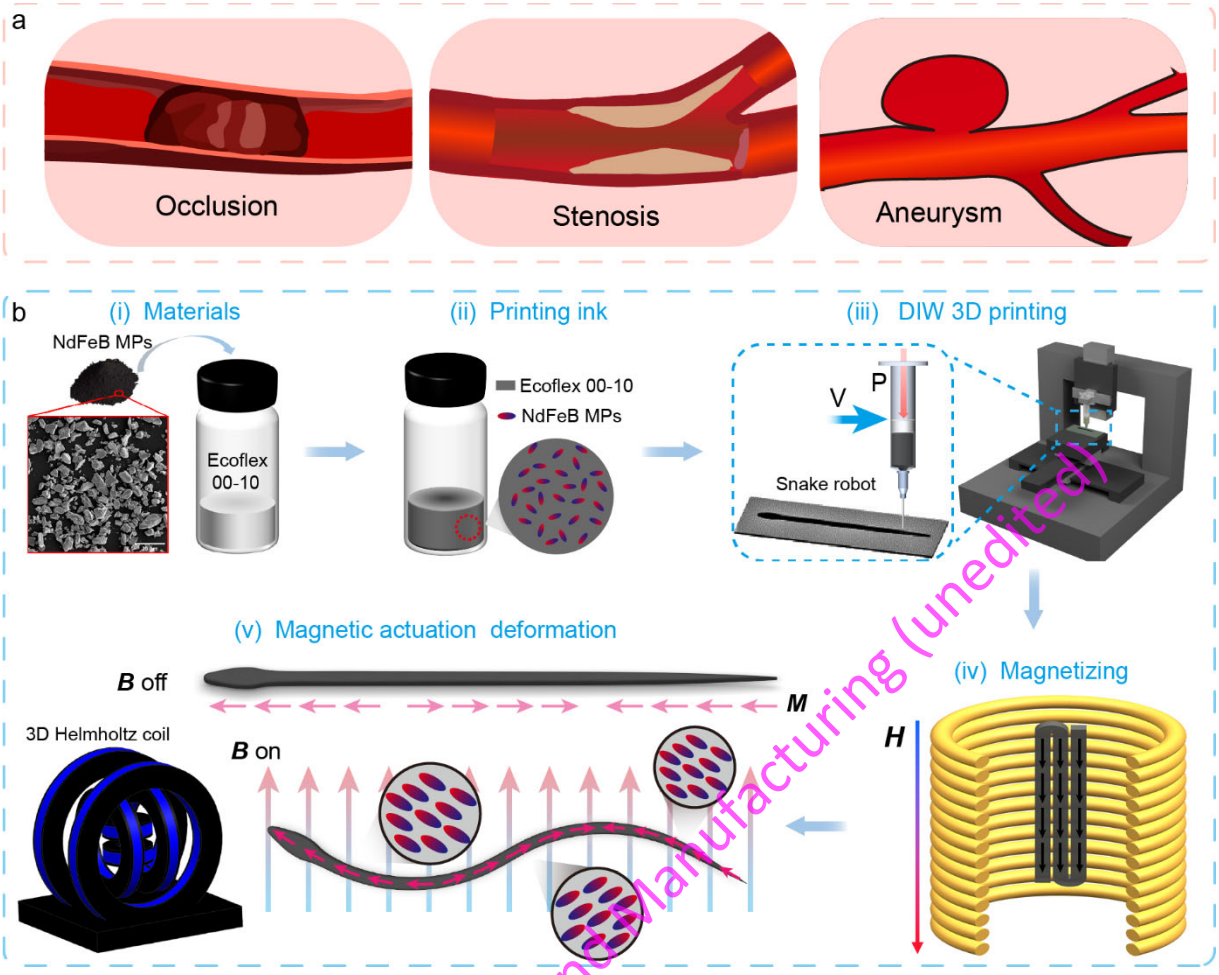

Fig. 1 Potential application scenarios of wireless micro-robots and schematic of the manufacturing process of the snake robot. **a** The pathological environment in human blood vessels is closed, narrow, tortuous, and liquid. **b** Schematic diagram of the manufacturing of snake robot. (i) Materials for magnetic responsive intelligent ink. (ii) Preparation of magnetic printing ink. (iii) Illustration of DIW 3D printing. (iv) 3D printed snake robot was folded and magnetized by a strong pulsed magnetic field. (v) Schematic of magnetic actuation deformation of 4D printed snake robot.

Experiments

Preparation of magnetic printing ink

NdFeB magnetic microparticles (Xiamen tungsten Technology Research Center; average diameter, 5 μm) were mixed evenly with the uncured polymer (Ecoflex 00-10, Smooth-On Inc.) in a mass ratio of 3:1. The ink was mixed using a planetary centrifugal mixer (ARE-310, Thinky) for 5 minutes at 2000 rpm and centrifuged for 3 minutes at 2200 rpm to remove air bubbles before printing.

Rheological measurement

The rheological properties of inks with different NdFeB content were measured by using a rotating rheometer (MCR302, Anton Paar) with a steel parallel plate (25 mm). Viscosity as a function of shear rate was measured by a steady-state flow test with a logarithmic sweep (0.001–100 s^{-1}) of shear rate. Shear storage modulus (G') and loss modulus (G") as a function of shear stress were measured by oscillating test at 1 Hz shear frequency logarithmic sweep shear stress (1-1000 Pa). The shear yield stress of each sample was determined as the shear stress when the shear and loss modulus are the same value. All rheological characterizations were performed at 25±3 °C, and the initial equilibrium time was 1 minute.

Optimization of printing parameters

Filaments were printed by adjusting the output air pressure of the distributor (120×7 kPa-240×7 kPa, with an interval of 30×7 kPa) and changing the printing speed (1-10 mm/s, with an interval of 1 mm/s). Each group of fine filaments was printed

with 5 strips. After the filament was cured, the fidelity of the printed filament was observed and its diameter was measured with an optical microscope. The optimum printing pressure and speed of the ink were determined according to the fidelity and diameter of the filament.

Soft millirobot fabrication

The self-built DIW 3D printer (AGS 1000, Aerotech) (Fig. S1) was equipped with a Z-axis stepping device, who can manipulate the height of the printing syringe up and down according to the printed layer thickness, and a gas distribution equipment (HP7x, EFD), who was used to extrude the ink through a micro nozzle (5132-0.25-b, EFD) with an inner diameter of 100 μm. The snake robot model was designed by Unigraphics NX (version 12.0). G-code commands were generated by slicing software Slic3r and imported into the control software (A3200 Motion Composer) to control the X, Y, and Z-axis stepper motors and the pressure distributor. After correcting the zero point, the printer deposited filaments layer by layer according to the printing path. Eventually, the snake robot was manufactured and cured at room temperature.

Preparation of drug mimetics and in vitro drug delivery

To encapsulate a drug in the head of a snake-like robot, a gelatin mixture with a mass ratio of 1:5:6 of gelatin, glycerol, and water (GGW) was prepared, boiled for 30 s, mixed, and heated to 80 °C until transparent. It was cast in a mould (DIW 3D printing) as the bottom layer, then the snake robot and Rhodamine B powder (Macklin, as a simulated drug) were placed in the mould and the gelatine mixture was cast again to cover them. After curing, the drug was wrapped around the robot's head by the mixture. The coronary intervention vascular model was immersed in warm water at 32 °C, and a rotating permanent magnet was used to induce a snake robot to swim to the target area in a fluctuating manner, waiting for the gelatin mixture to dissolve and release the simulated drug.

Magnetizing and actuation

The snake robot was magnetized with a capacitive pulse magnetizing and demagnetizing machine (DX-MAG-12C20, DEXINMAG China). The maximum voltage applied during magnetization was 1275 V, and the corresponding strong pulse magnetic field was 3.0 T, which was about twice the intrinsic coercive force of neodymium iron boron, enabling it to achieve saturation magnetization. Magnetically responsive intelligent materials could be used for a long time without demagnetization.

The magnetic actuation system consisted of a three-dimensional Helmholtz coil, a signal generator for controlling corresponding channels (CH1, CH2, CH3), three power amplifiers, and a PC terminal controller (Fig. S2). Among them, the Helmholtz coil was composed of three pairs of orthogonal customized electromagnetic coils, which was used to generate a three-dimensional magnetic field. The signal generator was controlled by software to generate a signal, and the current was output to the coil through a power amplifier, generating a sinusoidal magnetic field, a bias magnetic field, and a rotating magnetic field.

Actuation Analysis

A real-time motion monitoring system was established, which consisted of a high-speed camera (M120-16G-M, revealer) and corresponding real-time monitoring software. The camera was installed above the three-dimensional Helmholtz coil to take a top view of the snake-like robot. It had a frame rate of up to 2000 fps and could capture high-frequency oscillations. Open-source software (Tracker) was used to analyze captured videos and convert dynamic images into data. Except for special instructions, the origin of all analyzed coordinate axes was located at the vertex of the snake robot's head.

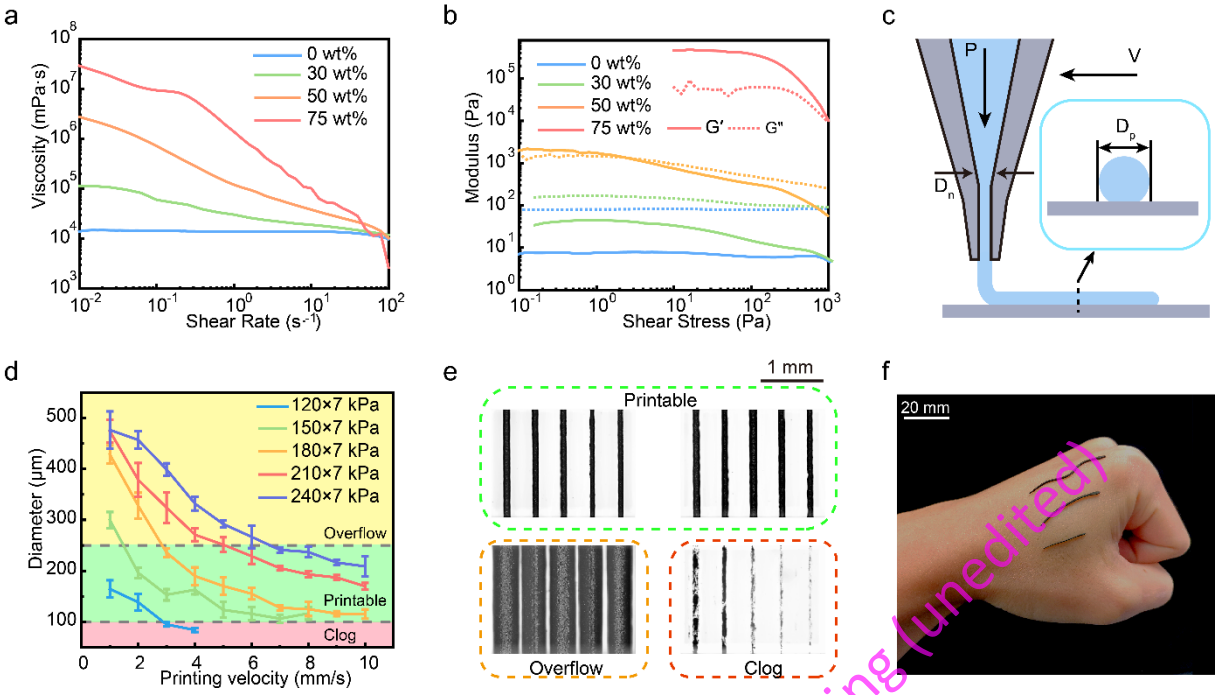

Fig. 2 Rheological properties and printing process parameters of magnetic responsive intelligent ink. **a** Viscosity of inks with the Ecoflex 00-10 and different NdFeB MPs contents. **b** Storage modulus and loss modulus of the inks. **c** Critical parameters of the DIW printing (applied pressure P, printing velocity V, nozzle diameter D_n, and printed filaments diameter D_p). **d** Line widths of different filaments printed by 75 wt% ink at different dispensing pressures P (120×7 kPa-240×7 kPa) and different printing velocities (1-10 mm/s). The inner diameter of the printing nozzle is 100 μm. **e** Optical microscope images of the filaments printed by 75 wt% ink at different printing parameters. **f** Three snake-like robots with various lengths on top of a hand shows the scale of a robot.

Results and Discussion

Design and manufacturing of snake biomimetic robot

Undulatory motion, a proven locomotion strategy in nature [39], inspired the development of a soft robot with a sleek, serpentine design. Employing optimized functional ink and advanced 3D printing techniques, this customizable robot features dimensions tailored for diverse environments (Fig. 1b). Achieving this required meticulous ink optimization to ensure smooth flow through fine deposition nozzles, promote high flexibility while maintaining robust magnetic torque, and provide ample structural integrity to withstand drying without delamination or distortion. To address these challenges, we developed an ink by blending microscale neodymium-iron-boron magnetic particles (NdFeB MPs) within a highly soft and stretchable silicone elastomer (Ecoflex 00-10), curable at room temperature, and this composite had been proven to be biocompatible [40]. The magnetic NdFeB particles were uniformly dispersed in the base material without precipitation or phase separation due to time variability (Fig. S3). The rheological properties of the inks could be finely tuned by adjusting the NdFeB MPs contents (Fig. 2a), with increasing magnetic particle content leading to a transition from a fluid to a paste state (Fig. 2b, Fig. S4), exhibiting desirable shear-thinning behavior ideal for printing. This thixotropic paste guaranteed optimal ink flow at high shear rates and shape stability at low shear rates, facilitating DIW 3D printing. Additionally, precise control over printing velocity and applied pressure was essential for achieving continuous filaments of defined diameters (Fig. 2c-e, Fig. S5), crucial for tailoring robots to specific specifications (Fig. 2f, Fig. S6). Through this optimization approach, we addressed challenges in robotic fabrication, paving the way for advancements in soft robotics and biomedical applications.

In harmony with the design, the magnetization intensity dwindles as the body extends further [41]. Capitalizing on the interplay of a dynamically oscillating magnetic field, the magnetic torque selectively engenders pronounced effects at the robot's head – the locus of maximal magnetization intensity. In stark contrast, the tail gracefully oscillates in a passive, fluctuating manner. This interplay begets a perpetual cascade of transverse oscillations, aptly channeling liquid motion. With this design, the combination of 4D printing technology and remote magnetic field manipulation bequeaths the robot with durability, flexibility, and most significantly, the unique ability to partake in autonomous swimming through the style of

undulatory propulsion. Optimized for anisotropic magnetization, the robot design ensured that the magnetic field predominantly impact the head, culminating in the desired wave-like motion.

Multiple wavenumbers of snake biomimetic robots

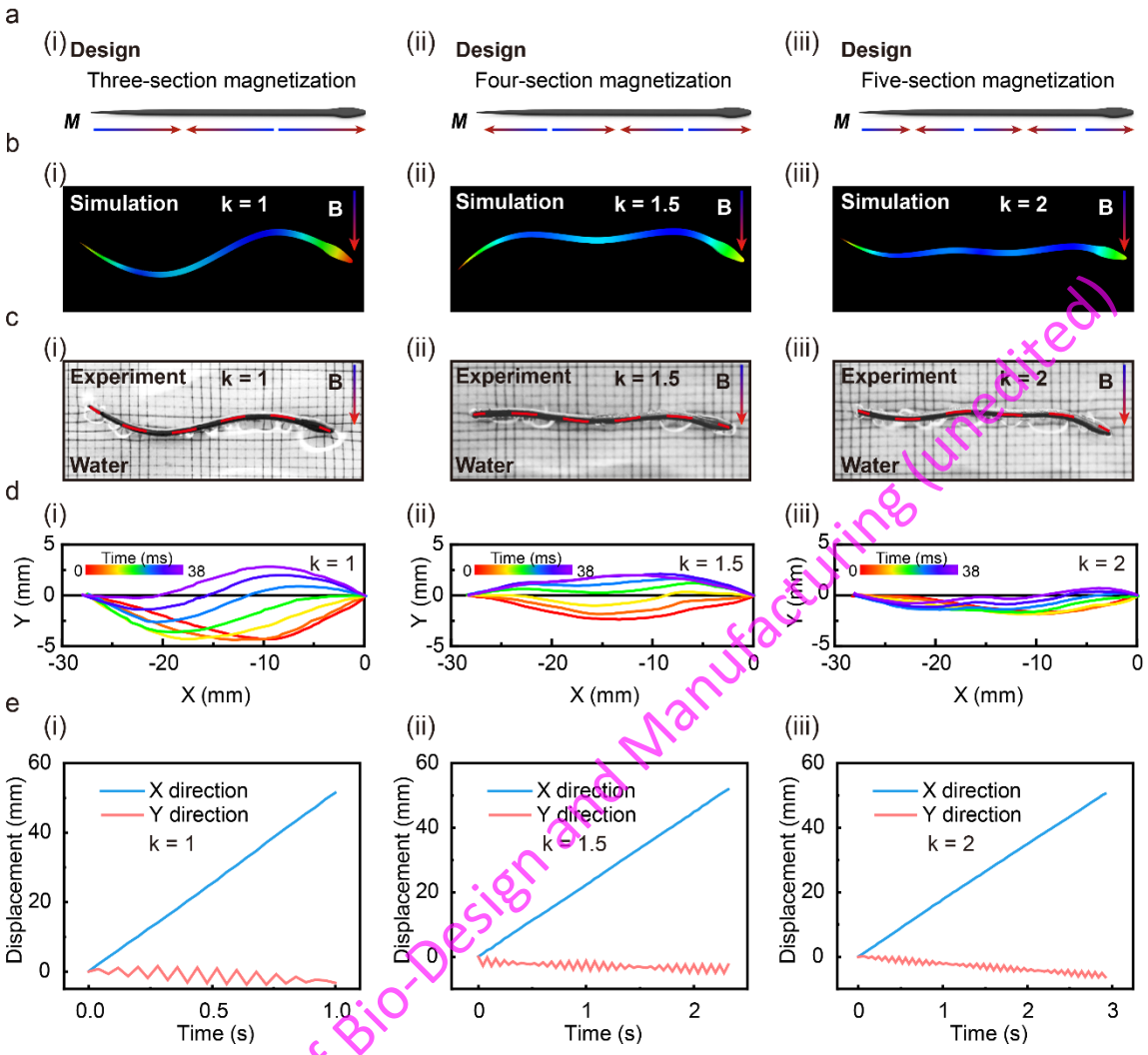

Fig. 3 Multiple wavenumbers of snake biomimetic robots. **a** Schematic diagram of snake robots with different magnetization directions for separate segments. (i) Three-section magnetization; (ii) Four-section magnetization; (iii) Five-section magnetization. **b** Simulation of snake robots generating deformations with different wavenumbers (k). (i) k = 1; (ii) k = 1.5; (iii) k = 2. **c** The snake robots distort at different wavenumbers under a magnetic field. **d** Swimming deformation sequence diagram of snake robots with different wavenumbers. As the wave number increases, the deformation amplitude of the robot decreases. **e** Swimming displacement of snake robots with different wavenumbers. The robot swims straight at a uniform speed, and as the wavenumber increases, the swimming speed decreases. Each square of the image background is 1 mm (the same below).

The snake robot was reshaped via magnetization, where different wavenumbers can be induced by applying the same magnetic field. The magnetization direction of the robot can be altered by folding it two, three, or four times (Fig. S7). Upon unfolding, the robot took on magnetization patterns characterized by three, four, or five distinct sections, respectively (Fig. 3a). To facilitate this design, a finite element analysis (FEA) model, as originally proposed by Zhao et al. [42, 43], was utilized to engineer the magnetic anisotropy of the snake robot, enabling the numerical simulation of its behavior within a magnetic field. Through simulations rooted in programmed magnetic anisotropy, we visualized the undulating body shapes of the magnetic robot with different wavenumbers (k = 1, k = 1.5, k = 2) (Fig. 3b). While minor variations in deformation amplitude may arise between simulation and experimental results, attributable to the difference in modeling mediums (FEA in air), the congruence in deformation patterns (Fig. 3c) underscores the efficacy of FEA in guiding the structural blueprint for magnetic deformations.

During the experiments, the swimming dynamics of the three distinct snake robots were analyzed by filming their motions throughout half-periods with a high-speed camera at 2000 frames per second. These recorded motions were then transformed into time-dependent shape curves (Fig. 3d). Notably, the snake robot with a 3-section magnetization exhibited significant undulatory deformations (Movie S1). As anticipated, an augmentation in the number of magnetization segments was met with a reduction in deformation amplitude, which in turn diminished the swimming velocity (Fig. 3e and Fig. S8). Importantly, the robot's displacement along the x-axis remained consistently linear, indicative of a constant swimming velocity. Although a minor deviation along the y-axis was observed, it was negligible when compared to the x-axis, reaffirming the robot's overall stability in maintaining linear motion.

Straight swimming of snake biomimetic robot

By controlling the output of the signal generator, a 3D Helmholtz coil generated different magnetic fields that actuated the magnetic snake robot to undergo desired deformations. In COMSOL Multiphysics, a sinusoidal current was fed into the Y-axis coil to output a periodic magnetic field (Movie S2). FEA was used for visualizing the magnetic field and assessing the spatial uniformity of the magnetic field ensconced within the coil (Fig. S9 and Fig. S10). Under the enchantment of this sinusoidal magnetic field, the head of the snake robot actively vibrated, while its body and tail passively swayed, producing undulations that enabled it to achieve self-propulsion (Fig. 4a (i)). Two distinct attributes governed this phenomenon. First, the robot's geometrical profile, gradually tapering from head to tail, begot a magnetic intensity gradient. The head, with the highest magnetic intensity, responded most emphatically to the magnetic field, precipitating maximum deformation (Fig. 4a (ii)). In stark contrast, the soft body and tail, with the lowest magnetic intensity, passively swayed (Fig. 4a (iii)). Hence, the head was always faster than the tail to reach its maximum deformation displacement (Fig. 4a (iv)). Second, magnetic anisotropy permeated the body, coaxing each segment to align with the magnetic field, transforming the otherwise elastic and malleable body into a sinuous, undulating form. Conjugating these attributes, the robot disseminated a procession of transverse waves along its body, thus scribing its narrative of self-propulsion (Movie S3).

The swimming velocity of robot was significantly influenced by the strength and frequency of the driving magnetic field, which surged with the intensification of the magnetic field, eventually yielding to a deceleration with increasing frequency of the magnetic field (Fig. 4b), reaching its zenith at an impressive 51.59 mm/s (1.705 BL/s, B = 14 mT, f = 13 Hz). The deformation amplitude was proportional to the magnetic field intensity (Fig. 4c and Fig. S11a), while the fluctuation displacement of the head along the Y-axis rose in tandem with magnetic field intensity (Fig. 4d), fostering greater body undulation and faster swimming velocity (Fig. 4h). Furthermore, the deformation of the robot in the magnetic field did not cause elastic damage, and it consistently maintained its initial deformation even after undergoing over 30,000 deformation cycles, indicating a dependable service life (Fig. S12).

Yet, frequency tempered this magnetic symphony. As the magnetic field frequency ascended, deformation amplitude regressed inversely (Fig. 4e), steadying into equilibrium beyond a certain frequency threshold (Fig. 4f). This heightened frequency intensified the robot's vibratory cadence but posed a challenge in synchronizing with the magnetic field's rapid tempo, leading to a drop in swimming speed and the occasional deviation from its intended course (Fig. 4i).

The snake robot's morphology adopted a vibratory style at lower frequencies (Fig. 4g and Fig. S11b), while its undulating motion yielded to disruption at higher frequencies. However, within the frequencies range of 11 to 17 Hz, the body generated prominent fluctuations for more efficient propulsion (Fig. S13). Last but not least, the robot's aquatic mobility was buoyed by its resilience against the viscous currents of diverse fluids (Fig. S14). In this challenging environment, the snake-shaped robot overcame the viscous resistance of liquids with different viscosities to achieve undulating swimming.

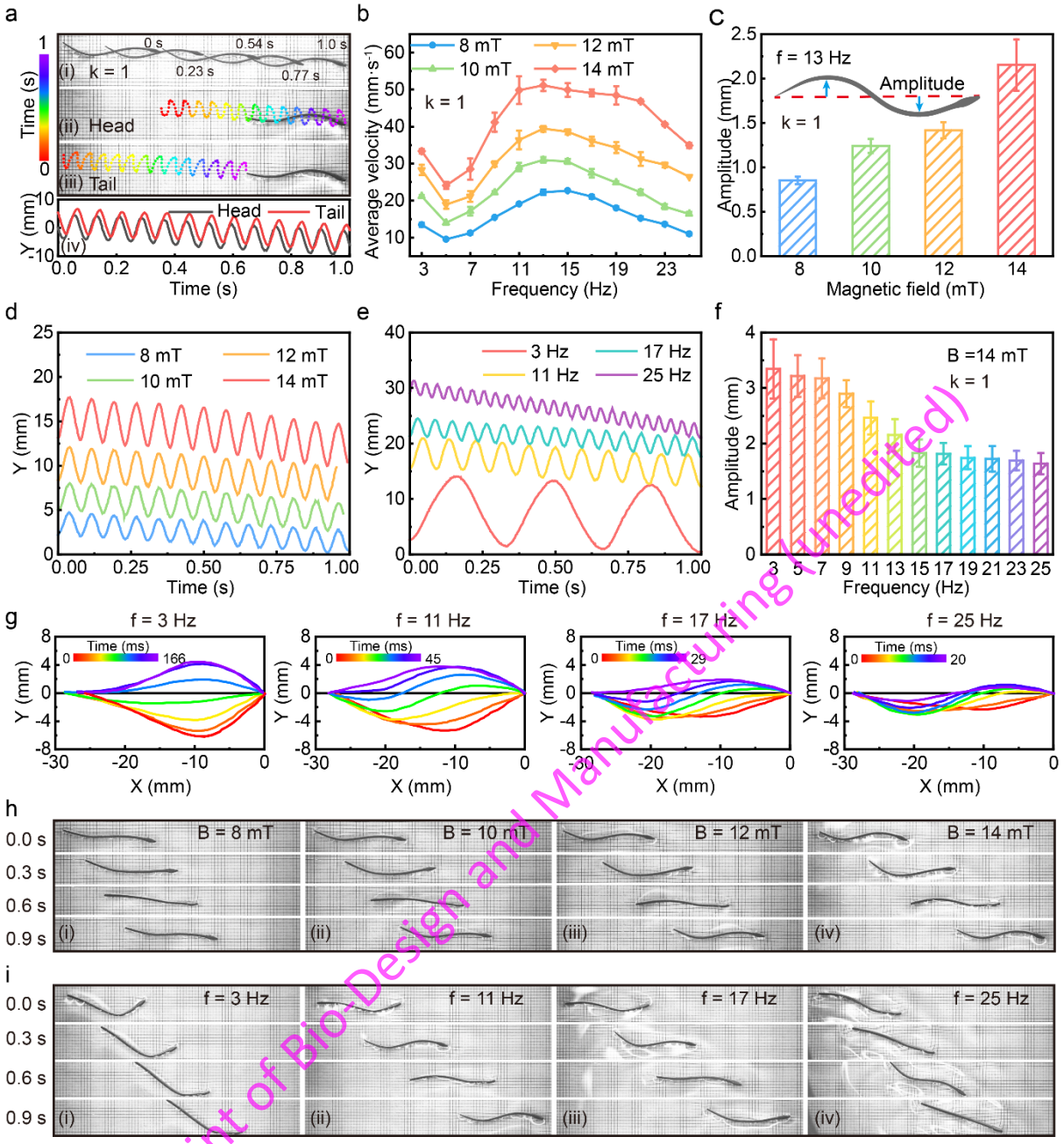

Fig. 4 Straight swimming of snake biomimetic robot. **a** Undulating swimming of a snake robot (B = 14 mT, f = 13 Hz). (i) Sequence diagram of a snake robot swimming in a straight line. (ii) The head swing trajectory diagram of the snake robot. (iii) The tail swing trajectory of the snake robot. (iv) Displacement diagram of the head and tail of the snake robot in the Y-axis direction over time. The head always reaches its maximum displacement before the tail, generating a series of waveforms that propagate along the body. **b** The influence of the intensities and frequencies of magnetic field on the swimming speed of the snake robot. The swimming speed rises as the magnetic field intensity increases and reaches its peak at medium frequencies. **c** The effect of magnetic field intensity on the deformation amplitude of the snake robot. **d** The head of a snake shaped robot oscillates under different magnetic field intensities. **e** The head of a snake shaped robot oscillates at different magnetic field frequencies. **f** The effect of magnetic field frequency on the deformation amplitude of snake robot. **g** Deformation sequence diagrams of snake robot at different magnetic field frequencies. **h** Swimming sequence diagram of a snake robot in different magnetic field intensities. **i** Swimming sequence diagrams of a snake robot at different magnetic field frequencies.

Turning swimming of snake biomimetic robot

When a robot ventures into a complex environment to execute its tasks, it invariably encounters intricate, meandering pathways. Thus, beyond the need for straightforward propulsion, it must possess the agility to execute precise turns as dictated by the circumstances. Magnetic robots offer advantages in multi-degree-of-freedom navigation, eliminating the need for

additional mechanisms components or actuators. This inherent flexibility renders them a highly attractive option for maneuvering through intricate and challenging terrains, akin to other driving techniques [44, 45]. Traditionally, the turning ability of most magnetic robots has relied upon aligning the net magnetic moment of the robot directly with the external magnetic field [46]. However, in a departure from conventional methodologies, the steering of our magnetic snake-shaped biomimetic robot is caused by asymmetric deformation induced by a biased sinusoidal magnetic field. The signal generator outputs a sinusoidal current, which at a moment t_0 transforms into a biased sinusoidal current, thereby generating a bias magnetic field. To gain insight into this intriguing process, COMSOL was enlisted to simulate the bias magnetic field for visual analysis (Fig. S15, Fig. S16 and Movie S2). Within a period, the magnetic field reached its peak on the biased side while diminishing on the opposite flank. At the precise juncture of t_0, the initially straight swimming snake robot, experienced asymmetric oscillations, leading to a turning motion (Fig. 5a and Movie S4). The robot attained maximal deformation on the side subjected to the stronger magnetic field, resulting in a directional shift. The magnitude of this turn augmented with the bias's intensification (Fig. 5d). It was noteworthy that under the influence of an unbiased magnetic field, the snake robot continued its linear trajectory without deviation.

Simultaneously, the application of a 90° phase-alternating current to the X-axis and Y-axis coils within a three-dimensional Helmholtz coil produced a magnetic field with phase differential. The convergence of spatial magnetic field vectors begot a rotatable magnetic field, with both direction and intensity being modifiable [47]. COMSOL played a pivotal role in the simulation, visualizing the rotating magnetic field (Fig. S17, Fig. S18 and Movie S2). This evolving magnetic field effortlessly coaxed the magnetization of the robot to continuously align with its rotational axis, ushering in a mesmerizing 360° circular trajectory and an uninterrupted alteration in swimming direction (Movie S5). Notably, the radius of the robot's circular trajectory remained consistently within the range of 15 mm and 20 mm, regardless of adjustments to the magnetic field intensity (Fig. 5b) or increases in frequency (Fig. 5c). This intriguing consistency highlighted that the robot's circular trajectory was relatively independent of magnetic field parameters. The utilization of cosine and sine magnetic fields generated by the X-axis and Y-axis coils respectively, can lead to the formation of either counterclockwise or clockwise rotating magnetic fields. The snake robot obediently followed suit, executing counterclockwise or clockwise circular swimming trajectories (Fig. 5e (i) and (ii)). By manipulating the magnetic field parameters, the motion of the snake robot can be precisely controlled, showcasing its flexibility in executing diverse swimming maneuvers.

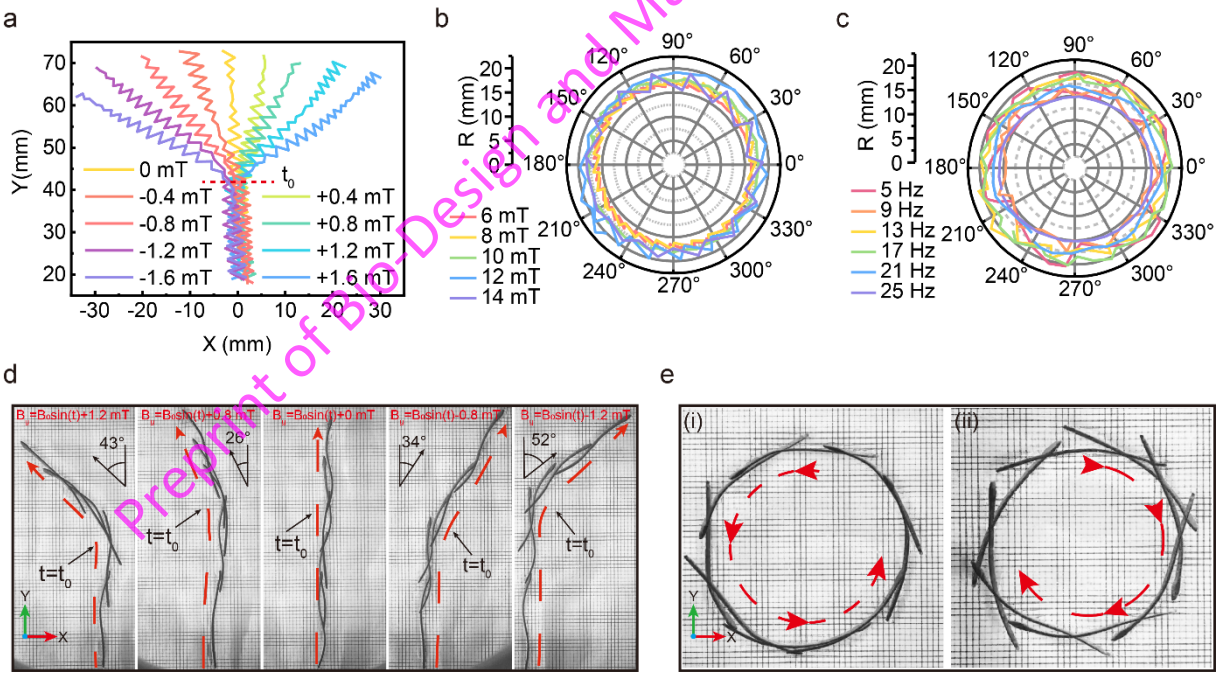

Fig. 5 Turning swimming of snake biomimetic robot. **a** The turning trajectory of a snake robot under different bias sizes of sinusoidal magnetic fields. As the bias size increases, the turning angle also exhibits a proportional increase. **b** Circular motion of a snake robot under different intensities of rotating magnetic fields. **c** Circular motion of a snake robot under different frequencies of rotating magnetic fields. **d** Turning sequence diagram of the snake robot. **e** Circular motion of a snake robot (B = 14 mT, f = 13 Hz). (i) Counterclockwise. (ii) Clockwise.

Collective and collaborative motion of snake biomimetic robots

Snake robots offer a distinctive advantage marked by their inherent flexibility and the ability to orchestrate collective behaviors (Movie S6). Interestingly, when compared to alternative propulsion methods, propelling multiple robots within the same operational zone does not incur greater power demands than driving a single robot under the equivalent magnetic field conditions [48, 49]. This trait assumes pivotal importance in scenarios where coordinated efforts are paramount, as a group of robots can efficiently transport a larger payload than a solitary unit [50]. Snake robot A, referred to as Robot A, effortlessly matched the forward swimming pace of Robot B (Fig. 6a and b), performing identical motions under the very same magnetic field conditions. Moreover, our fleet of snake robots included Robot C, with a thickness of 0.4 mm, and Robot D, boasting a more robust thickness of 0.8 mm. The distinction in their performances was palpable, with Robot D surging ahead at a markedly higher speed than Robot C (Fig. 6c and Fig. S19). A t = 0 s, Robot D lagged behind Robot C, but staged an overtaking maneuver in roughly 1 s (Fig. 6d).

Remarkably, snake robots are also adept at exhibiting cooperative behaviors. When two such robots were magnetically close together, the faster Robot D propelled the slower Robot C, fostering harmonious tandem swimming (Fig. 6e and Fig. S20a). Conversely, when Robot C was slower and trailed behind, the faster Robot D took the lead and pulled its slower partner to swim forward together (Fig. 6f and Fig. S20b). The synergy engendered during this collaborative swimming venture exerts a remarkable assistance effect, augmenting the swimming velocity of the slower robots by a substantial factor, ranging from 3.8 to 4.1 times their individual capabilities (Fig. 6g). This transformative effect underscored the value of cooperative behavior in achieving enhanced efficiency and productivity in diverse applications.

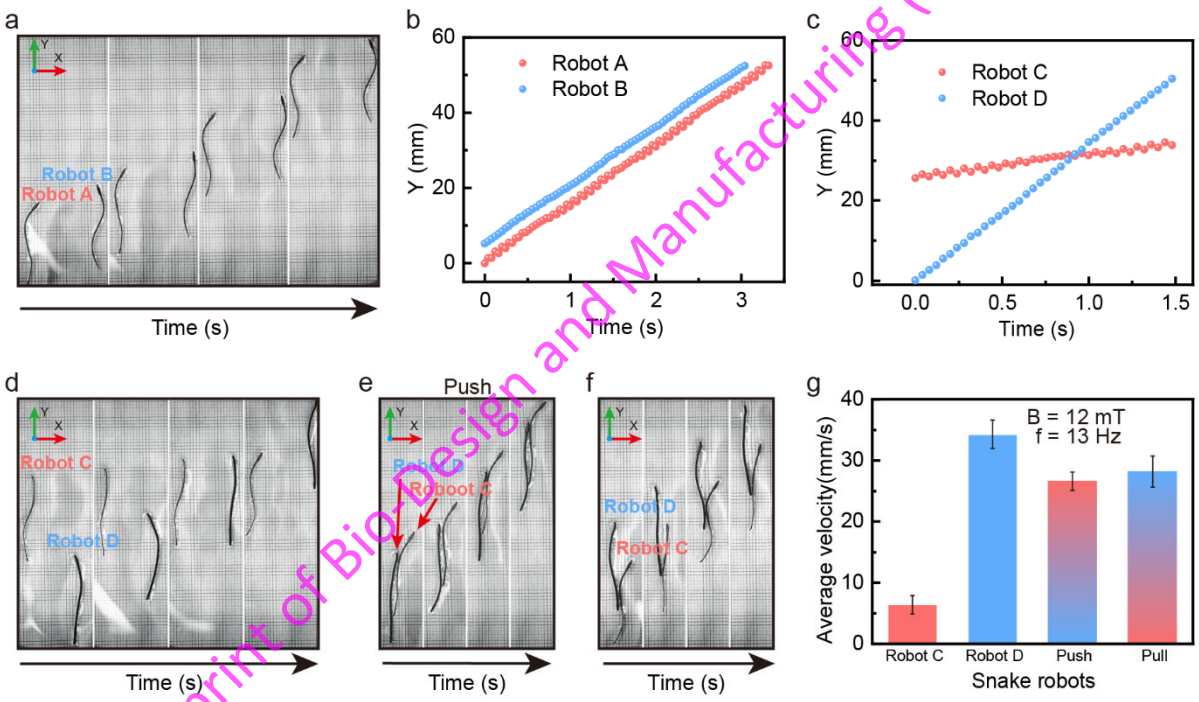

Fig. 6 Collective and collaborative motion of snake biomimetic robots. **a** Parallel swimming of snake robots. Snake robots A and B swam forward at the same speed. **b** The displacement of Robots A and B. **c** The displacement of Robots C and D. The speed of Robot C was slower than Robot D. **d** The sequence diagram of Robot D surpassing Robot C. **e** Robot D propelled Robot C to swim forward. **f** Robot D pulled Robot C to swim forward. **g** The individual and collaborative swimming speed of robots.

Navigation and drug release of snake biomimetic robot in vascular models

Medical conditions like ischemic stroke, myocardial infarction, and pulmonary embolism often necessitate treatment with drugs, administered either systemically or through local injections, to dissolve the blood clots [51, 52]. Among these treatments, recombinant tissue plasmin activator (rt-PA) stands out as a clot-dissolving drug with a well-established track record as the most effective intervention for acute ischemic stroke [53]. However, rt-PA has its limitations, including a short half-life of less than 10 minutes and the potential for bleeding complications during later stages of treatment [54]. This underscores the significance of targeted drug delivery systems, capable of circumventing these inherent challenges and enabling swift and precise drug administration at the desired location.

In this context, magnetic robots have emerged as novel delivery vehicles for drugs (Fig. 7a). The magnetic snake-like robot, proposed in this work, exhibited the capability to navigate narrow and tortuous blood vessels (Fig. S21). Characterized by its high aspect ratio and soft, pliable body, it generated substantial thrust for propulsion within the liquid environment. In addition, the ability to manipulate it remotely via magnetic fields (Fig. S22) granted it high agility within the confines of blood vessels (Fig. 7c, d and Movie S7). In order to carry cargoes, drugs (Rhodamine B was used in this article) can be securely wrapped in the head of the snake robot by a gelatin mixture (gelatin : glycerin : water = 1 : 5 : 6) (Fig. 7b). Notably, these components resembled the primary constituents of oral capsule shells, capable of gradual dissolution in warm water overtime, ensuring biodegradability [55]. Once the snake robot carrying drugs entered the blood vessel, it navigated swiftly and accurately to the target area. After 7 minutes, the gelatin mixture was completely dissolved in warm water (32 ℃), leading to a gradual drug dispersion across a wider region. (Fig. 7e and Movie S8). This drug release mechanism within the snake robot's design held significant promise for thrombolytic drug therapy. However, it's imperative to acknowledge that substantial efforts are still needed to refine and adapt this technology for practical use in real-world clinical settings.

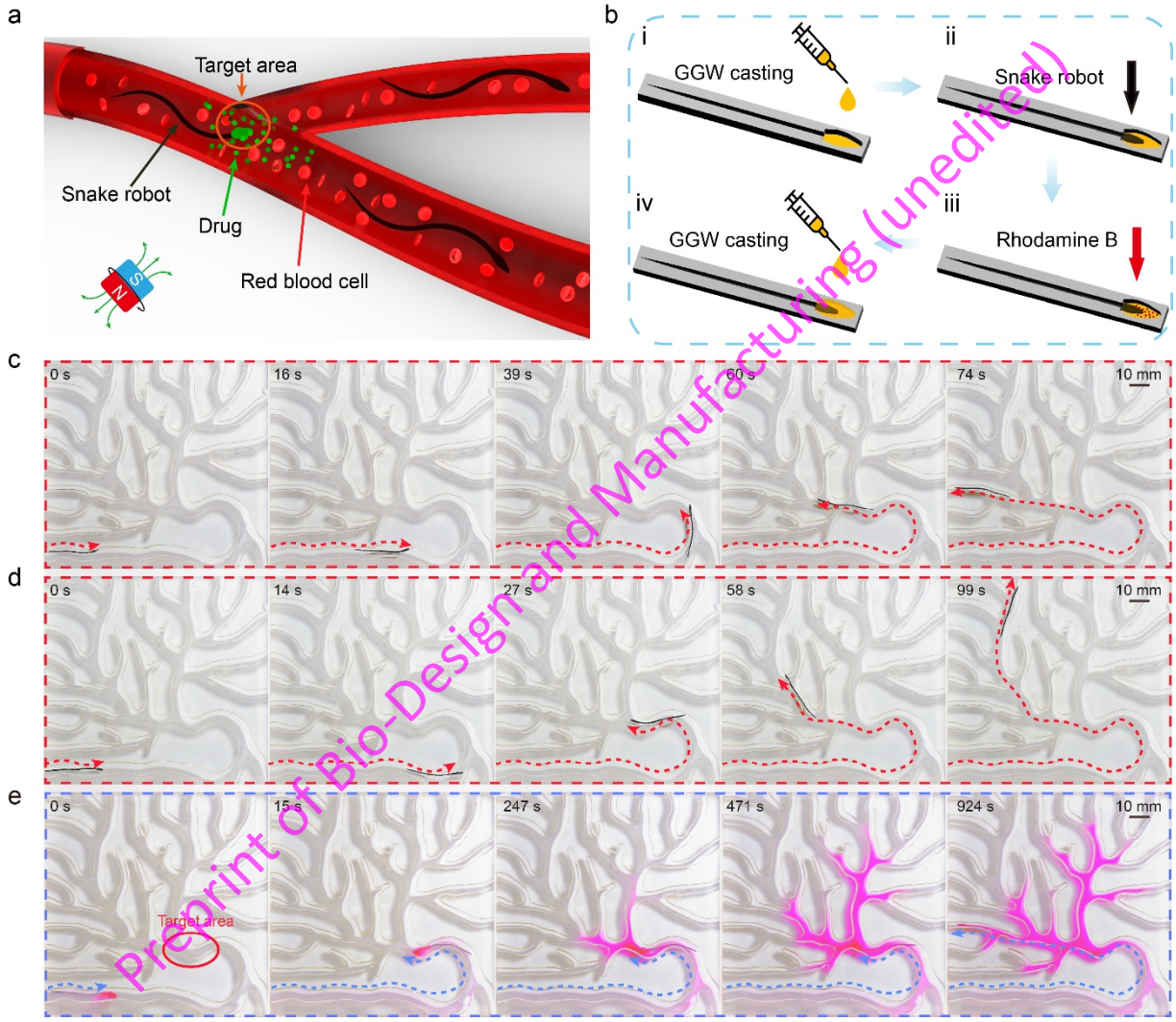

Fig. 7 Potential applications of the snake robot in the medical field. **a** Schematic diagram of snake robot releasing drugs in blood vessels. The drug is wrapped around the head of the robot and is released after reaching the target area under magnetic field. **b** Manufacturing of drug simulacrum wrapped around the robot's head. (i) The uncured GGW is cast in the mold as the bottom layer for encapsulating the drug. (ii) The snake robot is placed in the silicone rubber mold, (iii) Rhodamine B powder is placed in the head of the snake robot, (iv) and finally the uncured GGW is cast into the mold. After the GGW is cured, Rhodamine B is wrapped on the head of the snake robot. **c d** The snake robot navigates in a coronary intervention vascular model. After entering the vascular model, the snake robot navigates along a predetermined route. **e** The snake robot releases drugs in a coronary intervention vascular model. As a simulated drug, Rhodamine B was wrapped in the head of the snake robot by gelatin mixture. The snake robot stayed in the target area, and the gelatin mixture was dissolved in 32 ℃ warm water, waiting for the complete release of the drug.

Conclusions

In addressing the challenge of maneuvering soft robots through narrow biological passages for medical procedures, we introduce a novel wireless magnetic swimming snake-like robot. Engineered to navigate liquids using undulatory motion, this novel design combined a directly printable intelligent ink with 4D printing technology, enabling customizable thickness and streamlined fabrication of snake robots with diverse dimensions. Optimized for non-uniform magnetization, our robot effortlessly achieved snake-like undulatory motion at its head, akin to the fluid, straight swimming of natural serpents, propelling it to speeds of up to 51.159 mm/s (1.705 BL/s). Unlike magnetically driven robots relying on the steering style, the snake robot induced asymmetric deformation when subjected to a biased magnetic field. This interaction with the surrounding liquid prompted asymmetric reaction forces, which in turn led to precise steering capabilities. Furthermore, our snake robots exhibited cooperative behavior, significantly enhancing its swimming velocity when working in concert with its counterparts.

From the initial stages of fabrication via 4D printing to the diverse range of motion analyses conducted, snake robots had showcased significant contributions to the realm of biomimetic robotics. These contributions spanned from replicating shape characteristics to emulating flexible motion biomimetics. The elongated design not only generated effective self-propulsion but also allowed for rapid and precise drug release into narrow blood vessels, thereby facilitating targeted drug therapy for vascular diseases. The advent of this innovative technology held great promise and served as a source of inspiration for the application of biomimetic robots within medical domains, particularly in the context of vascular thrombolysis. Nevertheless, it's crucial to acknowledge that while these developments are promising, they must be tempered with the recognition that further research is needed to address the current limitations and challenges inherent to existing technologies.

Supplementary Information The online version contains supplementary material available at xxx

Acknowledgements The authors acknowledge funding from National Natural Science Foundation of China (No. 52105421, 52373050), Guangdong Provincial Natural Science Foundation (No. 2022A1515011621), Funding by Science and Technology Projects in Guangzhou (202102080330, 2024A04J6446). Supported by the Fundamental Research Funds for the Central Universities, Sun Yat-sen University (22qntd0101).

Author contributions XCO participated in conceptualization, investigation, methodology, formal analysis, investigation, and writing of the original draft. JQH and DTH were involved in supervision, conceptualization, writing—review and editing. XHL and GLC were involved in methodology. YY, RB and YS were involved in methodology, validation, and formal analysis. SZG contributed to conceptualization, funding acquisition, supervision, and writing—review and editing.

Declarations

Conflict of interest The authors declare that they have no known competing financial interests or personal relationships that could have appeared to influence the work reported in this paper.

Ethical approval This article does not contain any studies with human or animal subjects performed by any of the authors.

Reference

1. Peters BS, Armijo PR, Krause C, Choudhury SA, Oleynikov D (2018) Review of emerging surgical robotic technology. Surg Endosc 32:1636–1655. https://doi.org/10.1007/s00464-018-6079-2

2. Burgner-Kahrs J, Rucker DC, Choset H (2015) Continuum Robots for Medical Applications: A Survey. IEEE Transactions on Robotics 31:1261–1280. https://doi.org/10.1109/TRO.2015.2489500

3. Zhang H, Li Z, Gao C, Fan X, Pang Y, Li T, Wu Z, Xie H, He Q (2021) Dual-responsive biohybrid neutrobots for active target delivery. Sci Robot 6:eaaz9519. https://doi.org/10.1126/scirobotics.aaz9519

4. Wang B, Chan KF, Yuan K, Wang Q, Xia X, Yang L, Ko H, Wang Y-XJ, Sung JJY, Chiu PWY, Zhang L (2021) Endoscopy-assisted magnetic navigation of biohybrid soft microrobots with rapid endoluminal delivery and imaging. Sci Robot 6:eabd2813. https://doi.org/10.1126/scirobotics.abd2813

5. Ceylan H, Dogan NO, Yasa IC, Musaoglu MN, Kulali ZU, Sitti M (2021) 3D printed personalized magnetic micromachines from patient blood–derived biomaterials. Science Advances 7:eabh0273. https://doi.org/10.1126/sciadv.abh0273

6. Gu H, Möckli M, Ehmke C, Kim M, Wieland M, Moser S, Bechinger C, Boehler Q, Nelson BJ (2023) Self-folding soft-robotic chains with reconfigurable shapes and functionalities. Nat Commun 14:1263. https://doi.org/10.1038/s41467-023-36819-z

7. Yim S, Sitti M (2012) Design and Rolling Locomotion of a Magnetically Actuated Soft Capsule Endoscope. IEEE Transactions on Robotics 28:183–194. https://doi.org/10.1109/TRO.2011.2163861

8. Kim Y, Zhao X (2022) Magnetic Soft Materials and Robots. Chem Rev 122:5317–5364. https://doi.org/10.1021/acs.chemrev.1c00481

9. Nelson BJ, Kaliakatsos IK, Abbott JJ (2010) Microrobots for Minimally Invasive Medicine. Annual Review of Biomedical Engineering 12:55–85. https://doi.org/10.1146/annurev-bioeng-010510-103409

10. Sitti M (2018) Miniature soft robots — road to the clinic. Nat Rev Mater 3:74–75. https://doi.org/10.1038/s41578-018-0001-3

11. Nelson BJ, Kaliakatsos IK, Abbott JJ (2010) Microrobots for Minimally Invasive Medicine. Annu Rev Biomed Eng 12:55–85. https://doi.org/10.1146/annurev-bioeng-010510-103409

12. Jeon S, Hoshiar AK, Kim K, Lee S, Kim E, Lee S, Kim J, Nelson BJ, Cha H-J, Yi B-J, Choi H (2019) A Magnetically Controlled Soft Microrobot Steering a Guidewire in a Three-Dimensional Phantom Vascular Network. Soft Robotics 6:54–68. https://doi.org/10.1089/soro.2018.0019

13. Zhao X, Kim Y (2019) Soft microbots programmed by nanomagnets. Nature 575:58–59. https://doi.org/10.1038/d41586-019-03363-0

14. Lu H, Hong Y, Yang Y, Yang Z, Shen Y (2020) Battery-Less Soft Millirobot That Can Move, Sense, and Communicate Remotely by Coupling the Magnetic and Piezoelectric Effects. Advanced Science 7:2000069. https://doi.org/10.1002/advs.202000069

15. Haojian Lu, Mei Zhang, Yuanyuan Yang, Qiang Huang, Toshio Fukuda, Zuankai Wang, Yajing Shen (2018) A bioinspired multilegged soft millirobot that functions in both dry and wet conditions. Nat Commun 9:3944. https://doi.org/10.1038/s41467-018-06491-9

16. Gu H, Boehler Q, Cui H, Secchi E, Savorana G, De Marco C, Gervasoni S, Peyron Q, Huang T-Y, Pane S, Hirt AM, Ahmed D, Nelson BJ (2020) Magnetic cilia carpets with programmable metachronal waves. Nat Commun 11:2637. https://doi.org/10.1038/s41467-020-16458-4

17. Hu W, Lum GZ, Mastrangeli M, Sitti M (2018) Small-scale soft-bodied robot with multimodal locomotion. Nature 554:81–85. https://doi.org/10.1038/nature25443

18. Ren Ziyu, Zhang Rongjing, Soon Ren Hao, Liu Zemin, Hu Wenqi, Onck Patrick R., Sitti Metin (2021) Soft-bodied adaptive multimodal locomotion strategies in fluid-filled confined spaces. Science Advances 7:eabh2022. https://doi.org/10.1126/sciadv.abh2022

19. Ren Z, Hu W, Dong X, Sitti M (2019) Multi-functional soft-bodied jellyfish-like swimming. Nat Commun 10:2703. https://doi.org/10.1038/s41467-019-10549-7

20. Huang H-W, Uslu FE, Katsamba P, Lauga E, Sakar MS, Nelson BJ (2019) Adaptive locomotion of artificial microswimmers. Sci Adv 5:eaau1532. https://doi.org/10.1126/sciadv.aau1532

21. Wu Y, Dong X, Kim J, Wang C, Sitti M (2022) Wireless soft millirobots for climbing three-dimensional surfaces in confined spaces. Sci Adv 8:eabn3431. https://doi.org/10.1126/sciadv.abn3431

22. Wang T, Ren Z, Hu W, Li M, Sitti M (2021) Effect of body stiffness distribution on larval fish–like efficient undulatory swimming. Sci Adv 7:eabf7364. https://doi.org/10.1126/sciadv.abf7364

23. Liu Xinyue, Yang Yueying, Inda Maria Eugenia, Lin Shaoting, Wu Jingjing, Kim Yoonho, Chen Xiaoyu, Ma Dacheng, Lu Timothy K., Zhao Xuanhe (2021) Magnetic Living Hydrogels for Intestinal Localization, Retention, and Diagnosis. Advanced Functional Materials 31:2010918. https://doi.org/10.1002/adfm.202010918

24. Alapan Y, Yigit B, Beker O, Demirörs AF, Sitti M (2019) Shape-encoded dynamic assembly of mobile micromachines. Nat Mater 18:1244–1251. https://doi.org/10.1038/s41563-019-0407-3

25. Hakan Ceylan, Immihan Ceren Yasa, Oncay Yasa, Ahmet Fatih Tabak, Joshua Giltinan, Metin Sitti (2019) 3D-Printed Biodegradable Microswimmer for Theranostic Cargo Delivery and Release. ACS Nano 13:3353–3362. https://doi.org/10.1021/acsnano.8b09233

26. Lee Y-W, Ceylan H, Yasa IC, Kilic U, Sitti M (2021) 3D-Printed Multi-Stimuli-Responsive Mobile Micromachines. ACS Appl Mater Interfaces 13:12759–12766. https://doi.org/10.1021/acsami.0c18221

27. Yoonho Kim, German A. Parada, Shengduo Liu, Xuanhe Zhao (2019) Ferromagnetic soft continuum robots. Sci Robot 4:eaax7329. https://doi.org/10.1126/scirobotics.aax7329

28. Wang L, Guo CF, Zhao X (2022) Magnetic soft continuum robots with contact forces. Extreme Mechanics Letters 51:101604. https://doi.org/10.1016/j.eml.2022.101604

29. Dreyfus R, Boehler Q, Lyttle S, Gruber P, Lussi J, Chautems C, Gervasoni S, Berberat J, Seibold D, Ochsenbein-Kölble N, Reinehr M, Weisskopf M, Remonda L, Nelson BJ (2024) Dexterous helical magnetic robot for improved endovascular access. Science Robotics 9:eadh0298. https://doi.org/10.1126/scirobotics.adh0298

30. Kim Y, Genevriere E, Harker P, Choe J, Balicki M, Regenhardt RW, Vranic JE, Dmytriw AA, Patel AB, Zhao X (2022) Telerobotic neurovascular interventions with magnetic manipulation. Sci Robot 7:eabg9907. https://doi.org/10.1126/scirobotics.abg9907

31. Tiryaki ME, Elmacıoğlu YG, Sitti M (2023) Magnetic guidewire steering at ultrahigh magnetic fields. Science Advances 9:eadg6438. https://doi.org/10.1126/sciadv.adg6438

32. Mosauer W (1932) On the Locomotion of Snakes. Science 76:583–585. https://doi.org/10.1126/science.76.1982.583

33. Liu J, Tong Y, Liu J (2021) Review of snake robots in constrained environments. Robotics and Autonomous Systems 141:103785. https://doi.org/10.1016/j.robot.2021.103785

34. Virgala I, Kelemen M, Prada E, Sukop M, Kot T, Bobovský Z, Varga M, Ferenčík P (2021) A snake robot for locomotion in a pipe using trapezium-like travelling wave. Mechanism and Machine Theory 158:104221. https://doi.org/10.1016/j.mechmachtheory.2020.104221

35. Pettersen KY (2017) Snake robots. Annual Reviews in Control 44:19–44. https://doi.org/10.1016/j.arcontrol.2017.09.006

36. Thandiackal R, Melo K, Paez L, Herault J, Kano T, Akiyama K, Boyer F, Ryczko D, Ishiguro A, Ijspeert AJ (2021) Emergence of robust self-organized undulatory swimming based on local hydrodynamic force sensing. Sci Robot 6:eabf6354. https://doi.org/10.1126/scirobotics.abf6354

37. Sun Z, Zeng X, Deng X, Zhang X, Zhang Y (2023) Droplet interface in additive manufacturing: From process to application. Droplet 2:e57. https://doi.org/10.1002/dro2.57

38. Chen Jiayao, Liu Xiaojiang, Tian Yujia, Zhu Wei, Yan Chunze, Shi Yusheng, Kong Ling Bing, Qi Hang Jerry, Zhou Kun (2021) 3D-Printed Anisotropic Polymer Materials for Functional Applications. Adv Mater 2102877. https://doi.org/10.1002/adma.202102877

39. Choi H, Jeong S, Lee C, Park BJ, Ko SY, Park J-O, Park S (2014) Three-dimensional swimming tadpole mini-robot using three-axis Helmholtz coils. Int J Control Autom Syst 12:662–669. https://doi.org/10.1007/s12555-013-0378-0

40. Zhou C, Yang Y, Wang J, Wu Q, Gu Z, Zhou Y, Liu X, Yang Y, Tang H, Ling Q, Wang L, Zang J (2021) Ferromagnetic soft catheter robots for minimally invasive bioprinting. Nat Commun 12:5072. https://doi.org/10.1038/s41467-021-25386-w

41. Manamanchaiyaporn L, Xu T, Wu X (2020) Magnetic Soft Robot With the Triangular Head–Tail Morphology Inspired By Lateral Undulation. IEEE/ASME Transactions on Mechatronics 25:2688–2699. https://doi.org/10.1109/TMECH.2020.2988718

42. Zhao R, Kim Y, Chester SA, Sharma P, Zhao X (2019) Mechanics of hard-magnetic soft materials. Journal of the Mechanics and Physics of Solids 124:244–263. https://doi.org/10.1016/j.jmps.2018.10.008

43. Wang L, Kim Y, Guo CF, Zhao X (2020) Hard-magnetic elastica. Journal of the Mechanics and Physics of Solids 142:104045. https://doi.org/10.1016/j.jmps.2020.104045

44. Dong X, Kheiri S, Lu Y, Xu Z, Zhen M, Liu X (2021) Toward a living soft microrobot through optogenetic locomotion control of *Caenorhabditis elegans*. Sci Robot 6:eabe3950. https://doi.org/10.1126/scirobotics.abe3950

45. Qi X, Gao T, Tan X (2022) Bioinspired 3D-Printed Snakeskins Enable Effective Serpentine Locomotion of a Soft Robotic Snake. Soft Robotics. https://doi.org/10.1089/soro.2022.0051

46. Ze Q, Wu S, Dai J, Leanza S, Ikeda G, Yang PC, Iaccarino G, Zhao RR (2022) Spinning-enabled wireless amphibious origami millirobot. Nat Commun 13:3118. https://doi.org/10.1038/s41467-022-30802-w

47. Zhe W, Yang Y, Qiuliang W, Tao S (2008) A Novel Rotating Magnetic Field Generator for Driving Magnetic Micro-Machine. IEEE Transactions on Applied Superconductivity 18:887–890. https://doi.org/10.1109/TASC.2008.922243

48. Elgeti J, Winkler RG, Gompper G (2015) Physics of microswimmers—single particle motion and collective behavior: a review. Rep Prog Phys 78:056601. https://doi.org/10.1088/0034-4885/78/5/056601

49. Peyer KE, Zhang L, Nelson BJ (2013) Bio-inspired magnetic swimming microrobots for biomedical applications. Nanoscale 5:1259–1272. https://doi.org/10.1039/C2NR32554C

50. Pauer C, du Roure O, Heuvingh J, Liedl T, Tavacoli J (2021) Programmable Design and Performance of Modular Magnetic Microswimmers. Adv Mater 33:2006237. https://doi.org/10.1002/adma.202006237

51. Marti C, John G, Konstantinides S, Combescure C, Sanchez O, Lankeit M, Meyer G, Perrier A (2015) Systemic thrombolytic therapy for acute pulmonary embolism: a systematic review and meta-analysis. European Heart Journal 36:605–614. https://doi.org/10.1093/eurheartj/ehu218

52. Gurman P, Miranda O, Nathan A, Washington C, Rosen Y, Elman N (2015) Recombinant tissue plasminogen activators (rtPA): A review. Clinical Pharmacology & Therapeutics 97:274–285. https://doi.org/10.1002/cpt.33

53. Colasuonno M, Palange AL, Aid R, Ferreira M, Mollica H, Palomba R, Emdin M, Del Sette M, Chauvierre C, Letourneur D, Decuzzi P (2018) Erythrocyte-Inspired Discoidal Polymeric Nanoconstructs Carrying Tissue Plasminogen Activator for the Enhanced Lysis of Blood Clots. ACS Nano 12:12224–12237. https://doi.org/10.1021/acsnano.8b06021

54. Choi W, Cho H, Kim G, Youn I, Key J, Han S (2022) Targeted thrombolysis by magnetoacoustic particles in photothrombotic stroke model. Biomaterials Research 26:58. https://doi.org/10.1186/s40824-022-00298-y

55. Wang C, Puranam VR, Misra S, Venkiteswaran VK (2022) A Snake-Inspired Multi-Segmented Magnetic Soft Robot Towards Medical Applications. IEEE Robotics and Automation Letters 7:5795–5802. https://doi.org/10.1109/LRA.2022.3160753